Eng. & Technology, Vol.24, No.8, 2005

Strength Analysis of Delta Wing Structure With Different Configurations

Muhsin J. Jweeg,* Abbass Z. Salman**
Naseer H. Farhood**

Received on: 17/4/2005
Accepted on: 1/11/2005

Abstract

In this study, a theoretical analysis was used to investigate the wing aerodynamic analysis and the best structural configuration of a delta wing with a satisfaction for the design requirements.
The analysis was related with both the aerodynamic and structural design considerations such that, in the aerodynamic approach, an estimation of the pressure distribution and aerodynamic design characteristics of the wing in the supersonic potential flow was done by using low order panel method for different angles of attack. In the structural part, five geometric models of wing were tested for three types of aerodynamic loading by changing the angle of attack from (10-14)° by using the finite element technique to find stresses and deformations.
The results showed that a clear pattern of increasing peak pressure with angle of attack in agreement with increasing strength of the leading edge vortex. Also, the results showed that, the stresses generally decrease with increasing each of the thickness of wing shell, and number of spars and ribs chordwisely and spanwisely respectively. These results were compared with those of published data and it was found that they are accurate and reliable.

Keywords: Strength, Delta, Wing .

تحليل مقاومة هيكل الجناح المثلث لأشكال مختلفة

الخلاصة

لقد تم دراسة التحليل الأيروديناميكي والهيئة الهيكلية الأفضل لجناح طائرة مثلث الشكل في حالة الجريان فوق الصوتي مع تحقيق للمتطلبات التصميمية، تتعلق الدراسة بالاعتبارات التصميمية الأيروديناميكية والهيكلية معاً.
تم حساب توزيع الضغط والخواص الأيروديناميكية للجناح باستخدام طريقة الأشرطة لزوايا هجوم مختلفة في الجانب الايروديناميكي. أما في الجانب الهيكلي فقد تمت الدراسة باستخدام طريقة العناصر المحددة حيث فحصت خمسة نماذج هيكلية للجناح لثلاثة أنواع من الأحمال الأيروديناميكية بواسطة تغيير زوايا الهجوم من (10-14) درجة لإيجاد التشوهات والإجهادات نتيجة تأثير القوى الأيروديناميكية.
النتائج بينت بأن القيمة العليا للضغط تزداد مع زيادة زاوية الهجوم في توافق مع زيادة شدة الدوامات عند مقدمة الجناح بينما الإجهادات تقل بزيادة كل من سمك قشرة الجناح وعدد المقويات الطولية والعرضية على طول مطيار وباع الجناح على الترتيب. تم مقارنة هذه النتائج مع النتائج النظرية المماثلة لها ووجد تطابق جيد بينهما.

* College of Eng., Al-Nahrain University, Email: Muhsin j j @ Yahoo.com.
** Mechanical Eng. Dept, AL-Rasheed College of Eng. & Science, UOT.

https://doi.org/10.30684/etj.24.8A.16
2412-0758/University of Technology-Iraq, Baghdad, Iraq

Notations

A	Area of element	m^2
AR	Aspect ratio	-
[B]	Strain-Displacement Matrix	-
b	Wing span	-
C_r	Wing root chord	M
C_t	Wing tip chord	M
C_p	Pressure coefficient	-
(A_k, B_k, C_k)	Influence coefficient	m/N
E	Elasticity matrix	GPa
G	Shear modulus	GPa
k	Stiffness of wing	N/mm
$[k_e]$	Element stiffness matrix	N/mm
S_B	Boundary surface of wing	M
Re	Reynolds number	-
M	Mach number	-
u, v, w	Displacement field in x ,y, z	M
u'_i, v'_i, w'_i	Displacements along local coordinate	M
$U_\infty, V_\infty, W_\infty$	Free-stream potential components	m/s
X/C	Chordwise ratio of wing	-
Y/B	Spanwise ratio of wing	-
W	Weight of wing	Kg
Φ^*	Total potential	m/s
Φ_∞	Free-stream potential	m/s
Φ	Perturbation potential	m/s
ν	Poisson's ratio	-
α	Angle of attack	Degree
σ	Source strength	-
μ	Doublet strength	-
σ_y	Yield stress	MPa
σ_{von}	Von-misses stress	MPa
ξ, η, ζ	Intrinsic coordinate of shell elements	-
θ_x, θ_y	Rotation displacement components about local axes x′ and y′	Mm

Introduction

The general aerodynamic shape structure is required to support two distinct classes of loading, the first, termed ground loads that are encountered by aircraft during movement and transportation on the ground, while the second is the air loads imposed on the structure during flight by environmental conditions.

The wing is the most important part in aircraft, which is responsible for producing the lift and supporting the aircraft in the air. The function of

the wing structure is to transmit and resist the applied loads, to provide an aerodynamic shape and to protect the contents of structure from the environment conditions encountered in flight. The wing shell is usually stiffened by longitudinal stringers and transverse ribs to enable it to resist bending, axial, shear, and twisting loading, [1]. The structure is known as semi-monocoque, figure (1).

Therefore, the structural analysis is essential for calculation the displacements and stresses by using numerical method, such as finite element method since the analytical approach contains many assumptions due to the complexity of the wing structure. the configuration surface is approximated by a set of panels on which unknown "singularity strengths" are defined. Boundary conditions are imposed at a discrete set of points, such as panel centers, there by generating a system of linear equations relating the singularity strengths which established the properties of the flow, [2].

The whole configuration of wing structure is composed of a large assemblage of various structural elements such as beams, plates and shells or a combination of them. Their overall geometry becomes extremely complex and can not be represented by a single mathematical expression, but by representing each of the above elements with the used finite element method and applying boundary conditions after the aerodynamic loading are imposed in the structural mesh then, the analysis is simplified for the solution by using MSC/NASTRAN documented package to reach for the final results, [3].

In this paper, the procedure of analysis was completed by selecting the best compromise that meets both structural consideration (high strength to weight ratio and high stiffness to weight ratio at specified mesh point of the structure) with nominal performance criteria at the worst case ($Re=8\times10^6$, $M=2.2$, and $\alpha=14°$) as well as the other angles of attack for each design and finally comparing the weights of these various designs to find the best choice, and this was achieved by using NASTRAN program version (2.2).

Aerodynamic Investigation

Delta wing configuration for the Dassault-Brequet Mirage III_E aircraft was chosen in the present work as a case study. The following description refers to the above aircraft wing. Cantilever low-wing monoplane of delta planform, with conical camber. Thickness to the chord ratio 3.5-4.5 %, no incidence, sweep back on leading-edge 60° 34'. All metal torsion-box structure stressed skin of machined panels with integral stiffeners, [5 and 6]. Further details are listed below:

Span	8.22 m
Aspect ratio	1.94
Length overall	15.03m
Height overall	4.5 m
Gross area	34.85 m^2
Airfoil section	64A-004(mod.)
Geometric shape	Delta
Tip chord	0.576 m
Root chord	7.21 m
Taper ratio	0.08
Mean aerodynamic chord	3.605 m
Max. Level speed	Mach 2.2
A/C weight empty	7000 kg
Max. Wing loading	393 kg/m^2

Panel Method

The low order panel method is based on the surface distribution of singularity elements then the surface is subdivided into a large number of panels each of which contains an aerodynamic singularity distribution. A system of linear equations relating the strengths of the singularities to the magnitude of the normal velocities induced of special control points to be made. The singularity strength that satisfies the boundary condition of the tangential flow at the control points for a given Mach number and a given angle of attack are determined by solving this system of equations. This approach seems to be more economical in the computational than the other numerical techniques employed such as finite difference methods.

Basic Formulation

The basic formulation will be based on reference, [7]. Consider Fig.(2), the velocity potential "Φ^*" is superimposing of:

a. Free stream.
b. Source distribution.
c. Doublet distribution.

The continuity equation must satisfy the Lap lace's equation:

$$\nabla^2 \Phi^* = 0 \qquad ...(1)$$

The general solution by Green's identity is the sum of source "σ" and doublet "μ" distributions, placed on the boundary S_B

$$\Phi^*(x,y,z) = \frac{-1}{4\pi}\int_{S_B}\left[\sigma\left(\frac{1}{r}\right) - \mu\vec{n}\cdot\vec{\nabla}\left(\frac{1}{r}\right)\right]ds + \Phi_\infty \qquad ...(2)$$

Where:

$\vec{n}$: Normal vector directed towards the flow field, normal to the body.

$\Phi_\infty = U_\infty x + V_\infty y + W_\infty z$ Free stream potential ...(3)

Since a large number of source and doublet distributions will satisfy a given set of boundary conditions, therefore, an arbitrary choice has to be made in order to select the desirable combination of such singularity elements. To uniquely define the solution of this problem, two problems must be introduced. First, an arbitrary decision has to be made in regard to the "right" combination of source and doublet distributions. Secondly, some physical considerations need to be introduced in order to fix the amount of circulation around the surface S_B. These considerations have led to the introduction of a wake model and fixation of its orientation and geometry. It is likely that the wake will be modeled by thin doublet or vortex sheets Fig. (2), thus, equation (2) can be re-written as:

$$\Phi^*(x,y,z) = \frac{1}{4\pi}\int_{body+wake}\mu\,\vec{n}.\vec{\nabla}\left(\frac{1}{r}\right)ds - \frac{1}{4\pi}\int_{body}\sigma\left(\frac{1}{r}\right)ds + \Phi_\infty \qquad ...(4)$$

The Boundary Conditions

The boundary conditions of zero flow normal to the surface must be applied. It can be specified as follow:

A. Neumann Boundary Condition

In this case $\partial\Phi^*/\partial n$ is specified on the solid boundary;

$$\vec{\nabla}(\Phi + \Phi_\infty).\vec{n} = 0 \qquad ....(5)$$

Here Φ is the perturbation potential and Φ_∞ is the free-stream velocity potential. The second boundary condition requires that the flow

disturbance at distance far from the body should be diminished,

$$\lim_{r\to\infty} \vec{\nabla}\Phi = 0 \qquad \ldots(6)$$

Where, r is the radial distance from the body. To satisfy the boundary condition in Eq. (5) directly, the velocity field due to the singularity distribution of Eq. (2) is used:

$$\nabla\Phi^*(x,y,z) = \frac{1}{4\pi}\int_{body+wake}\mu\,\vec{\nabla}\left[\frac{\partial}{\partial n}\left(\frac{1}{r}\right)\right]ds - \frac{1}{4\pi}\int_{body}\sigma\,\vec{\nabla}\left(\frac{1}{r}\right)ds + \vec{\nabla}\Phi_\infty \qquad \ldots(7)$$

Substitution of Eq. (7) into the B.C. in Eq. (5) results in:

$$\left\{\frac{1}{4\pi}\int_{body+wake}\mu\,\vec{\nabla}\left[\frac{\partial}{\partial n}\left(\frac{1}{r}\right)\right]ds - \frac{1}{4\pi}\int_{body}\sigma\,\vec{\nabla}\left(\frac{1}{r}\right)ds + \vec{\nabla}\Phi_\infty\right\}.\vec{n} = 0 \qquad \ldots(8)$$

This equation is the basis for many numerical solutions and should be hold for every point on the boundary S_B.

B. Dirichlet Boundary Condition

In this case, the perturbation potential Φ has to be specified everywhere on the boundary S_B. By using Equation (4)

and, $\vec{\nabla}(\Phi+\Phi_\infty).\vec{n} = 0$ or

$\Phi_i^* = (\Phi+\Phi_\infty)_i = const.$

$$\Phi_i^*(x,y,z) = \frac{1}{4\pi}\int_{body+wake}\mu\,\frac{\partial}{\partial n}\left(\frac{1}{r}\right)ds - \frac{1}{4\pi}\int_{body}\sigma\left(\frac{1}{r}\right)ds + \Phi_\infty = const \qquad \ldots(9)$$

Equation (9) is the basis for methods utilizing the indirect boundary conditions. If this equation is solved for $\Phi_i^* = 0$, then the resulting singularity distribution will include.

Verification Case

In order to be sure about the reliability of the program performance, a comparison study was made for the sweep delta wing of a 60° for both chordwise and spanwise directions for the upper surface subjected to pressure load with the angle of attack 10° at M=2.2 with altitude H=12km. The results of the pressure distribution are shown in figures 3 a, and b which agree fairly well compared with the results obtained by, [8].

Finite Element Method

Element Selection

The common types of elements employed for the static analysis of wing structure are shown in figure (4) that is implemented in the finite element principles.

The wing shell, ribs, and spar web are modeled by using the quadrilateral 8-node shell element, while the spar flange is modeled as a beam element.

The combined membrane-flexural element has five degrees of freedom at each node as Ahmed, Irons and Zienkiewicz element [9], three translations in the nodal x, y and z directions and two rotations a bout the nodal x and y axes. The materials to be used were the isotropic Al-Alloys which contribute in aerospace structure due to their high strength to weight and high stiffness to weight ratios. The properties of materials used are shown in table (1).

Description of the Geometric Modeling

In this work, five finite element models are created for the purpose of studying the effect of the structure of wing portions on its response under the action of the design loading that

occurred during critical flight conditions. The construction steps of the model are as follows:

i. The geometric domain of the wing aerodynamic shape is considered as skin surface joins the root and tip airfoils, in addition to interior surfaces represent the geometric domain of spars and ribs stiffeners. The boundary curves of each of the root and tip airfoil, spar, and rib surfaces are defined through eight located points. The skin surface is created as a ruled surface between the root and tip airfoil curves, while each of the spars and ribs surfaces are created as edge surface within the boundaries of their corresponding curves.

ii. The skin surface is discretized into high-order shell elements of quadrilateral shape, such that the mesh density is discretized into twenty one segments along airfoil sections, and fifteen segments along span direction as shown in mesh generation Fig.(5). Each of the spars surfaces are discretized into fifteen high-order shell elements of quadrilateral shape, while each of the rib surfaces is discretized into nineteen high-order shell elements of quadrilateral shape and another two shell elements of triangular shape.

The structure description of first model will be shown in details in figure (6) and for all of these models, the thickness values for the selected wing elements are illustrated in table (2).

Validity of Using NASTRAN/ Ver.2.2 Program

In order to demonstrate the accuracy of the NASTRAN/ Ver.2.2 program presented in this work, a comparison study was carried out for a pinched cylinder problem which was analyzed as given in reference, [10].

The parameters subjected to the cylinder are the load P=450N, radius of cylinder 12.58cm, length of the cylinder 26.289cm, E=72.4GPa, v=0.321, and the skin of cylinder is 0.238cm and only one half of the shell need to be analyzed due to the symmetry. The obtained maximum deformation showed a good agreement. See figure (7).

Finite Element Grid	Ref. [10] "Deflection under the Load" [× 0.0254]	NASTRAN "Deflection under the Load" [× 0.0254]
4×8	0.0245m	0.0242m

Results and Discussions

The structural considerations and weights for all the five created models are shown in tables (3and4) with changing of the aerodynamic load at α = (10-14°) such that the first design shows high safety factor (1.37), strength to weight ratio (1.39)MPa /kg, and stiffness to weight ratio (9.33×10^{-3}) 1/kg.m with a minimum mass of 337kg even with high aerodynamic load at α = 14°. Tables (5-8) illustrate the effect of skin thickness and material type variation on the wing strength with the mass calculation for each design case (skin thickness 0.001m gives maximum stress ratio of 73.5% and mass of 239.4kg for Al-Alloy 7075-T6), while for Al-Alloy 2024-T3 at the same thickness of 0.001m,the stress ratio is 110% i.e. out of failure with a mass of 238kg. Table (9) shows that the Al-Alloy 7075-T6 material for this design is the best one. Figures (12-15) show the pressure distribution along chordwise and spanwise of wing so

that the pressure distribution which indicate a clear pattern of increasing peak pressure coefficient value with increasing angle of attack, for instant from (-0.189 to 0.5) at $\alpha = 10°$ to (-0.275 to0.64) at $\alpha = 14°$.

Finally, Figs. (16-24) show the Von-Misses, max. shear, and max. principal stresses along chordwise and spanwise of wing for all the designed models at various aerodynamic loading according to the angle of attack. Also, these figures exhibit the deflection values along spanwise of wing.

Conclusions

From the discussions of the obtained results for aerodynamic and structural studies, the following points may be concluded.

1. The pressure distribution shows a clear pattern of increasing peak pressure with angle of attack, in agreement with the increasing strength of the leading edge vortex.
2. The comparison between the results obtained for all the designed models of wing structure showed that the parameters of first design were better than others in spite of using high aerodynamic loading (gave minimum stress ratio of 73% with higher strength and stiffness to weight ratios of 1.39MPa/kg and 9.33×10^{-3} 1/kg.m respectively for the worst case of pressure loads ($\alpha=14°$).
3. The obtained results with the aerodynamic load at angle of attack equals to 10° were more stable than the others especially in regard to the deflection values for each of the designed configurations, because of at high angles of attack such as $\alpha=14°$ or more, the wing situation approaches the stalling condition.
4. Using the aluminum alloy 7075-T6, for both stiffeners and skin and the 10×6 configuration with skin thickness equal to 0.0025m gives better safety factor estimated according Von-Misses theory, higher strength to weight ratio with an equivalent weight of wing structure rather than using the duralumin 2024-T3 with the same specifications (the 7075-T6 resulted in 55.4%(i.e. S.F=1.8), 1.217MPa/kg and 386kg, while the 2024-T3 resulted in 82.5%(i.e. S.F=1.2), 0.835MPa/kg and 383kg for the stress ratio, strength to weight ratio and total mass respectively).

References

1. Rivello, R.M., Theory and Analysis of Flight Structures Mcgraw-Hill Book Company, New York, 1969.
2. Davenpart, F.J., "Singularity Solution To General Potential Flow Airfoil Problems" Boeing Airplane Co., Report No, D6, 7202, 1981.
3. Erdener, O., "Development of Structural Model of A Fighter Wing", Ph.D. Thesis, Department of Aeronautical Engineering, Virginia Tech, September 2002.
4. Megson, T.H.G., Aircrat Structures For Engineering Students First Published By Edward Arnold (Publishers) Ltd 41 Bedford Square, London, 1985.
5. Paul, J., Janes of Aircrats Pergamon Press, New York, 2000.
6. Jone, J. B. . Michael, L. S., Aerodynamics For Engineering Prentice-Hall Inc., Upper Saddle River, New Jersey, 1998.
7. Woodward, F.A., "An Improved Method For The Aerodynamics Analysis of Wing-Body-Tail

Configuration In Subsonic And Supersonic Flow" Part I, NASA CR-2228, 1984.

8. Zohar, Y. Er-El, J. " Influence of The Aspect Ratio On The Aerodynamics of The Delta Wing At High Angle of Attack " J. Aircraft 25, Pp. 200–205, 1992.
9. Ahmad, S., Irons, B.M., Zienkiewicz, O.C. "Analysis of The Thick and Thin Shell Structures By Curved Finite Elements" Int. J. Number. Methods Eng., Vol. 3, No. 4, Pp.575-586, 1980.
10. Raju, I.S. . Prakasa, R. "Conical Shell Finite Element" Computer and Structures, Vol. 4, Pp. 901-915, 1984.
11. Murphy, A.J. Materials In Aircrat Structures Centenary J. Roy. Aero. Soc., 1866-1966.
12. Weaver, W. Jr. . Johnston, P.R. Finite Elements For Structural Analysis Prentice-Hall, Englewood Cliffs, N.J., 1987.

Table (1) The Properties of the Material Used in Aircraft Structure [11]

Material	Young Modulus (GPa)	Yield Stress (MPa)	Poisson's ratio	Density (kg/m^3)	Shear Modulus (GPa)	Ultimate Stress (MPa)
7075-T_6	73	470	0.33	2800	27.5	630
2024-T_3	74	320	0.33	2770	27.8	479

Table (2) The Thickness of Wing Design Models

Thickness (mm)	Model 1	Model 2	Model 3	Model 4	Model 5
Wing Skin	2	2	2	3	3
Middle Spar	4 Spars of 5	2 Spars of 5	2 Spars of 5	------	------
Auxiliary spar	3	3	3	3	3
Main Spar	-----	-----	-----	2 Spars of 10	3 Spars of 10
Ribs	3	3	3	3	3

Table (3) Comparison Criteria among the Designed Configurations

Aerodynamic load With (α) Equal To	Model No.	Stress Ratio $\left(\frac{\sigma_{von}}{\sigma_{yield}}\right)$	Strength to Weight Ratio $\left(\frac{\sigma_y}{W}\right)$ (MPa/kg)	Stiffness to Weight Ratio $\left(\frac{k}{W}\right)\times 10^{-3}$ (1/kg.m)
14°	M_1	0.73	1.39	9.33
	M_2	0.80	1.23	4.12
	M_3	1.29	1.32	2.86
	M_4	0.9	0.94	2.90
	M_5	0.79	0.88	3.10
12°	M_1	0.54	1.39	17.50
	M_2	0.53	1.23	6.10
	M_3	0.86	1.32	4.30
	M_4	0.60	0.94	4.36
	M_5	0.53	0.88	4.64
10°	M_1	0.32	1.39	22.0
	M_2	0.32	1.23	10.3
	M_3	0.51	1.32	7.16
	M_4	0.36	0.94	7.28
	M_5	0.31	0.88	7.73

Table (4) Masses for the wing designed models

Wing design	Model 1	Model 2	Model 3	Model 4	Model 5
Masses (kg)	337	383	355	498	532

Table (5): The effect of skin thickness (Design 1 - α=14°), Material: Al-Alloy (7075-T6), Density: - 2800 Kg/m³, Configuration: - 10 × 6

Model No.	Skin Thickness (m)	Displacement (m)	V.M. Stress (MPa)	Stress Ratio
16	0.001	0.318	345.7	73.50%
17	0.0015	0.286	314.6	67.00%
18	0.002	0.257	286	60.80%
19	0.0025	0.231	260.5	55.40%
20	0.003	0.208	237	50.40%

Table (6) Calculation of Masses

Model No.	Skin Thickness (m)	Masses (kg)			Wing total mass (kg)
		Skin	Spars	Ribs	
16	0.001	97.4	108	34	239.4
17	0.0015	146.2	108	34	288.2
18	0.002	194.8	108	34	337
19	0.0025	243.6	108	34	386
20	0.003	292.0	108	34	434

Table (7): The effect of material type (Design 1 - α=14°), Material: - Al-Alloy (2024-T3), Density: - 2770 Kg/m3, Configuration: - 10 x 6

Model No.	Skin Thickness (m)	Displacement (m)	V.M. Stress (MPa)	Stress Ratio
21	0.001	0.320	350.4	110%
22	0.0015	0.289	318	99.0%
23	0.002	0.260	290	90.6%
24	0.0025	0.233	264	82.5%
25	0.003	0.210	240	75.0%

Table (8) Calculation of Masses

Model No.	Skin Thickness (m)	Masses (kg)			Wing total mass (kg)
		Skin	Spars	Ribs	
21	0.001	96	108	34	238
22	0.0015	144.6	108	34	286.6
23	0.002	192.8	108	34	334.8
24	0.0025	241	108	34	383
25	0. 003	289	108	34	431

Table (9) Comparison of Materials,
Configuration: - 10 x 6, Skin thickness: - 0.0025 (m)

Material	Displacement (m)	V. M. Stress (MPa)	Stress Ratio	Wing Total Mass (kg)	Strength to Weight Ratio (MPa/ kg)
7075-T6	0.231	260.5	55.4%	386	1.217
2024-T3	0.233	264.0	82.5%	383	0.835

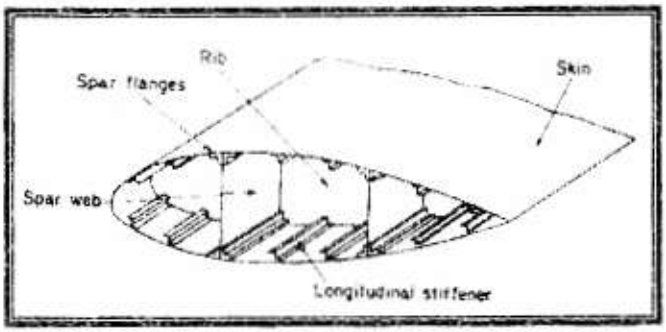

Fig.(1) Structural Arrangement for a Wing [4]

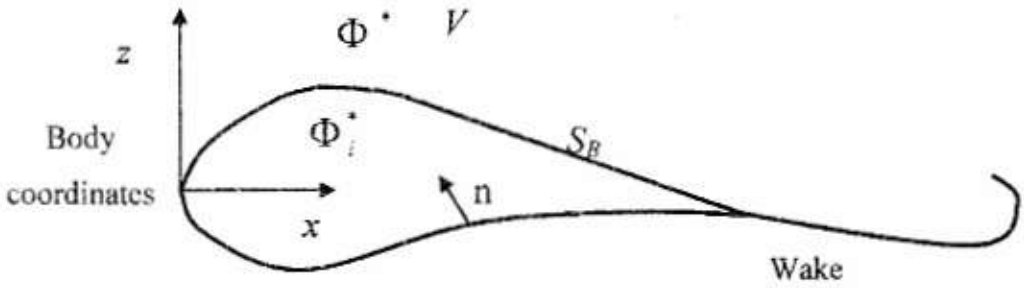

Figure (2) Potential Flow over a Closed Body

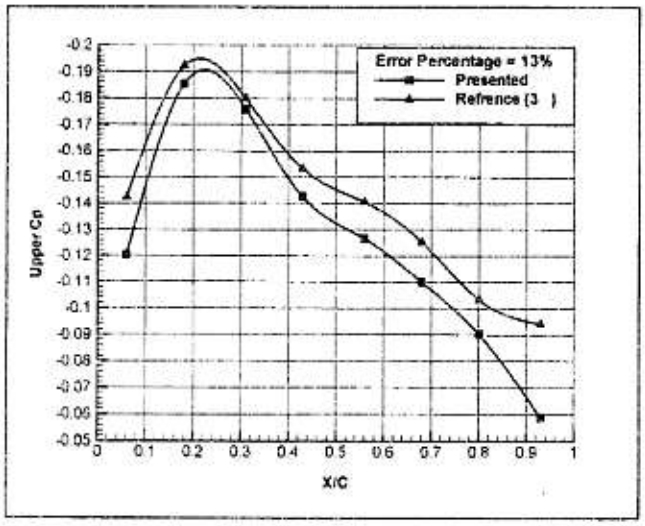

Fig. (3-a) Chordwise Pressure distribution at mean aerodynamic chord $\alpha = 10^{\circ}$

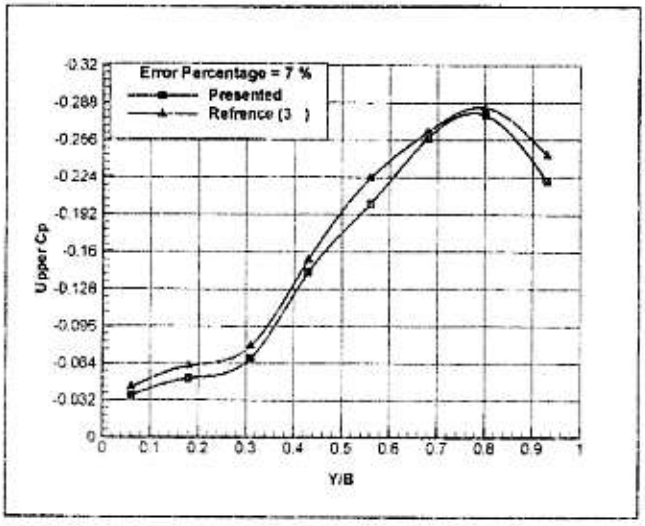

Fig.(3-b) Spanwise pressure distribution at 45% of root chord on lee-side of a 60° sweep delta wing

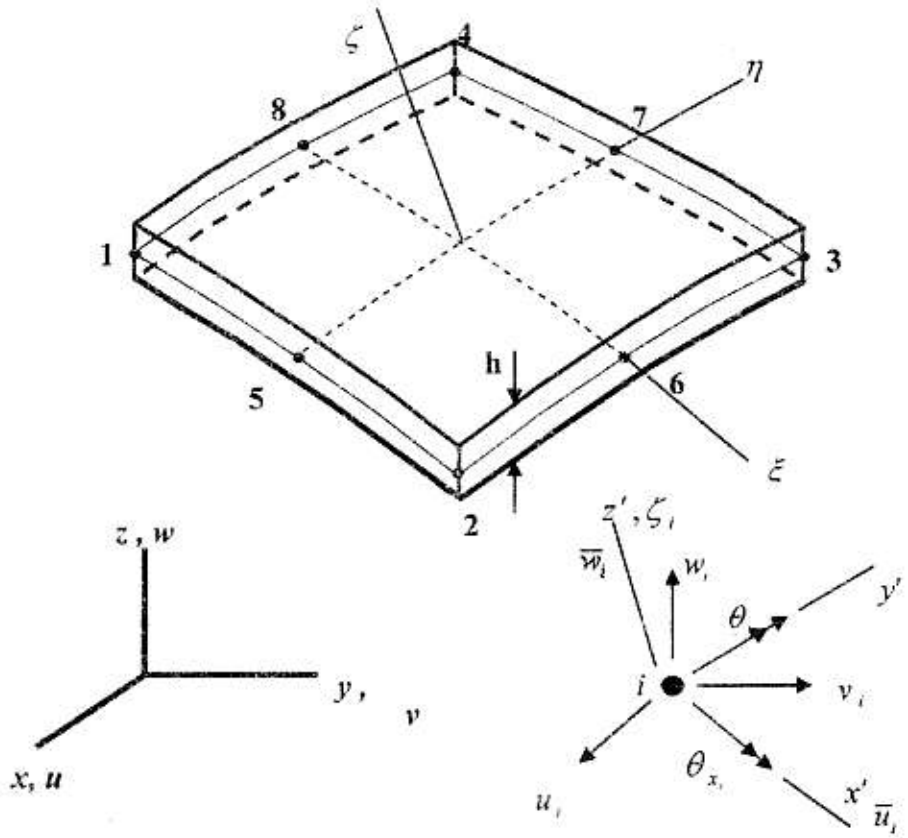

Figure (4) "Element SHQ8" Isoparametric quadrilateral shell element 8 nodded [12]

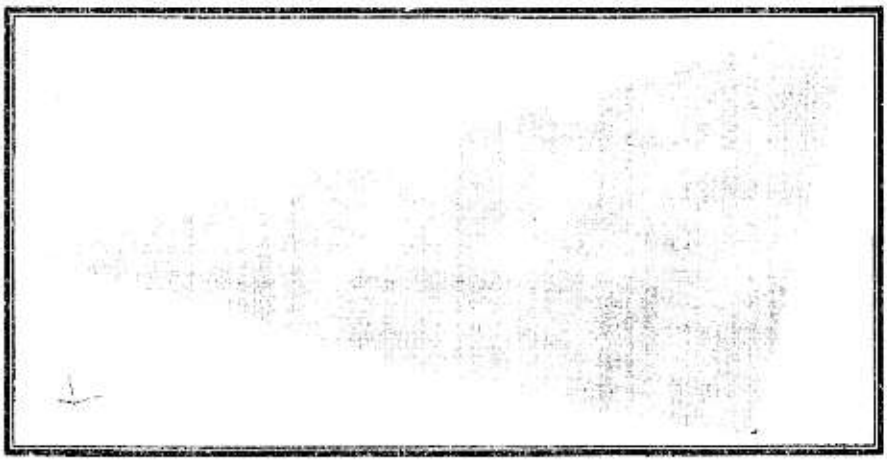

Fig.(5) Discretization of the geometry for a wing

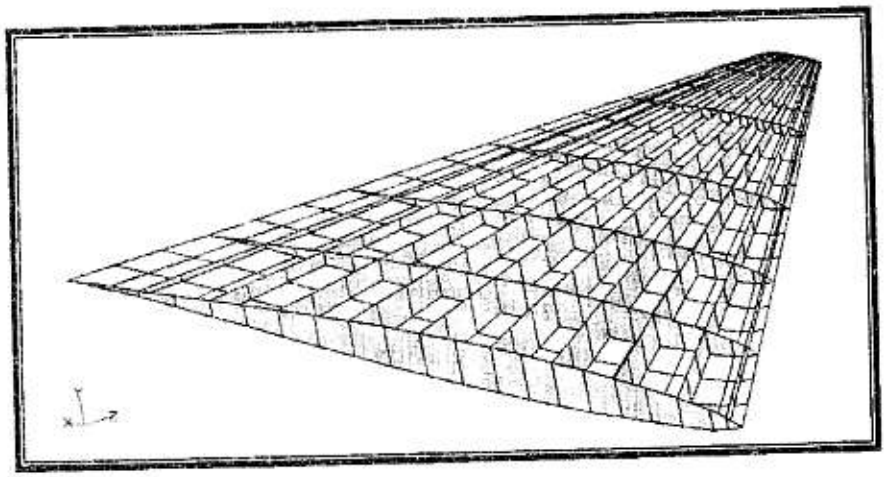

Fig.(6) The wing finite element model 1

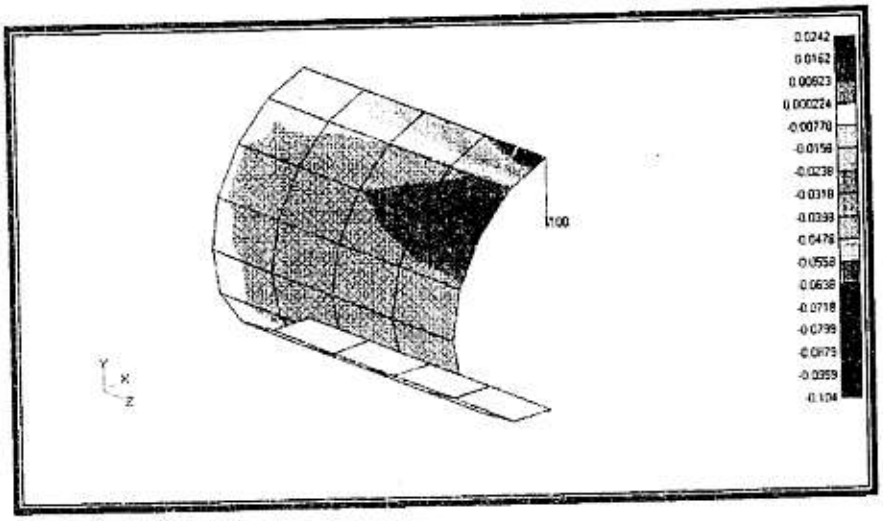

Fig.(7) Deflection (m) under the load obtained by MSC/NASTRAN (× 0.0254)

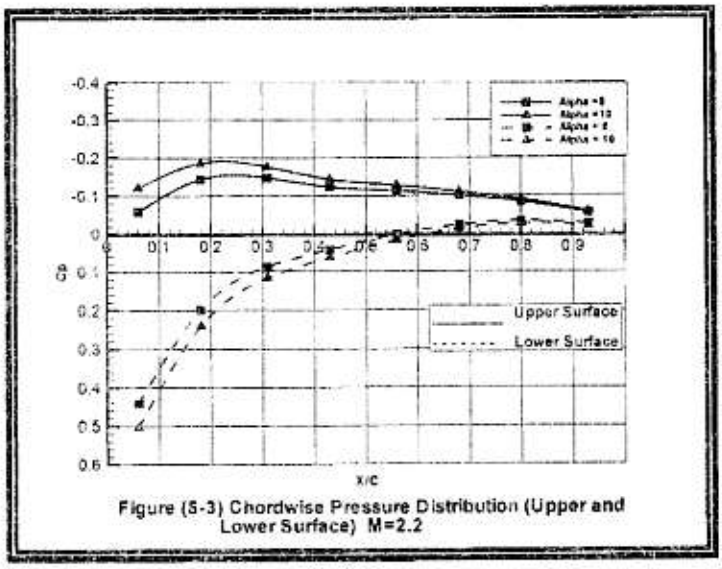

Figure (5-3) Chordwise Pressure Distribution (Upper and Lower Surface) M=2.2

Fig. (8) Chordwise Pressure distribution (upper and Lower surface) M=2.2

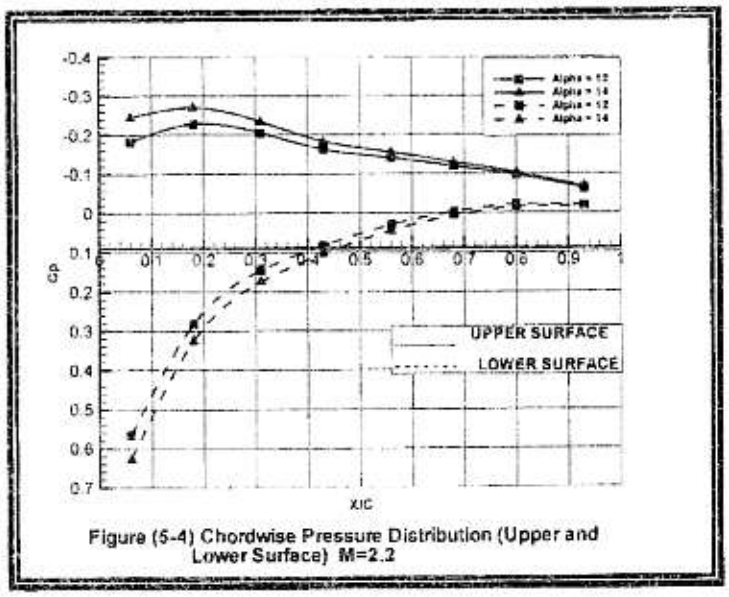

Figure (5-4) Chordwise Pressure Distribution (Upper and Lower Surface) M=2.2

Fig. (9) Chordwise Pressure distribution (upper and Lower surface) M=2.2

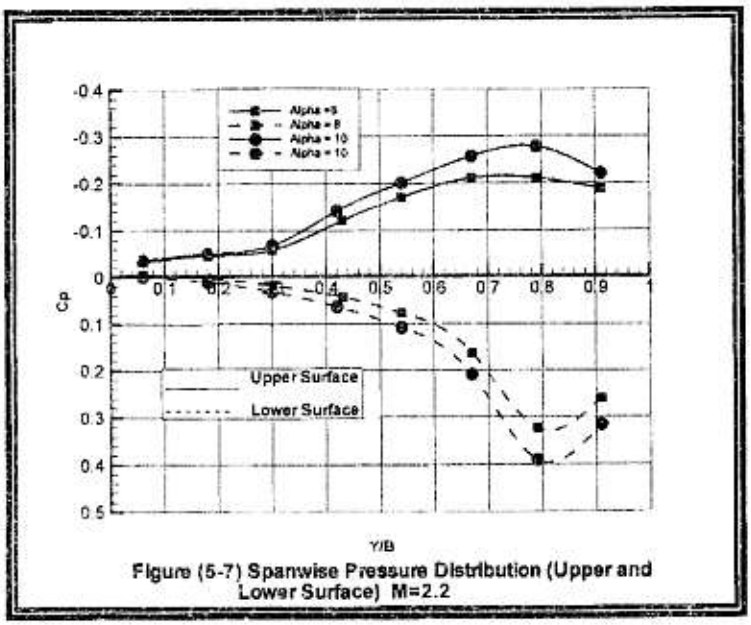

Fig. (10) Spanwise Pressure distribution (Upper and Lower surface) M=2.2

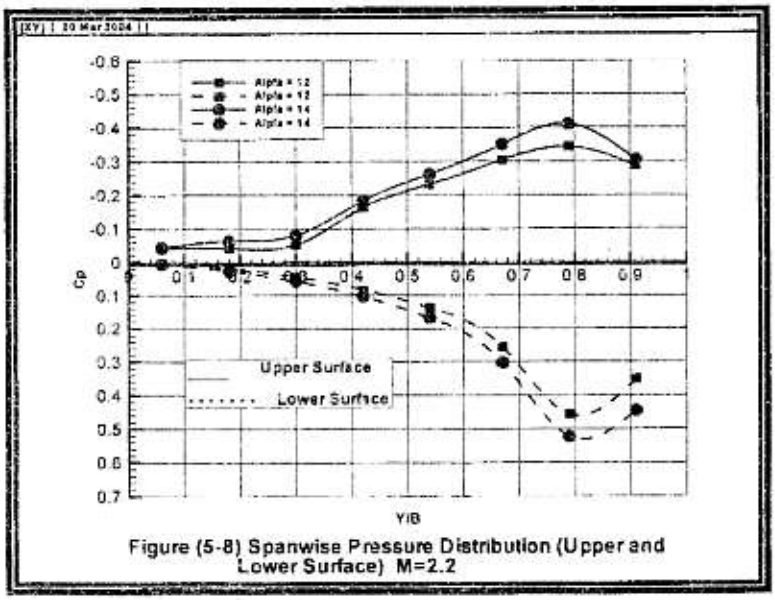

Fig. (11) Spanwise Pressure distribution (Upper and Lower surface) M=2.2

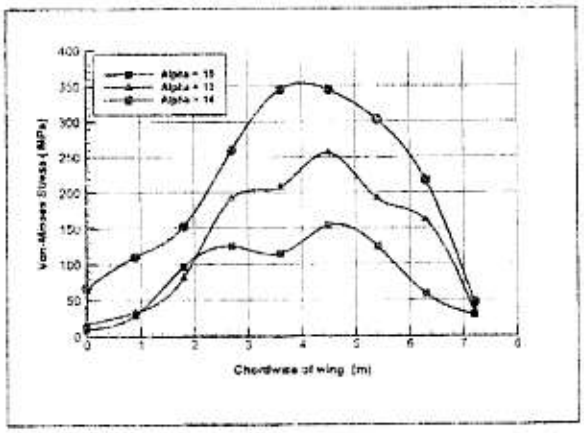

Fig. (12) Von-Misses stresses Vs chordwise (x) of wing design 1

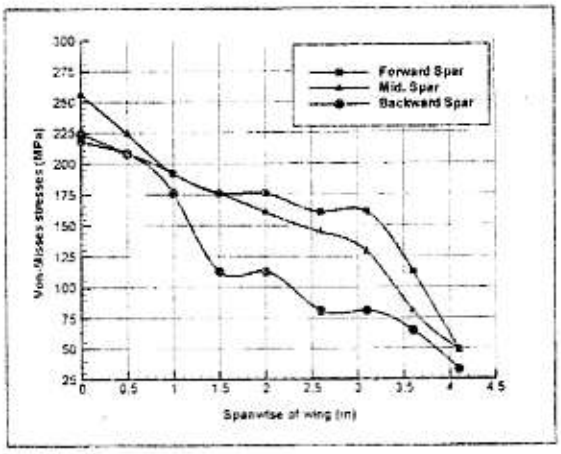

Fig. (13) Von-Misses stresses Vs spanwise (y) of wing design 1 (α=12°)

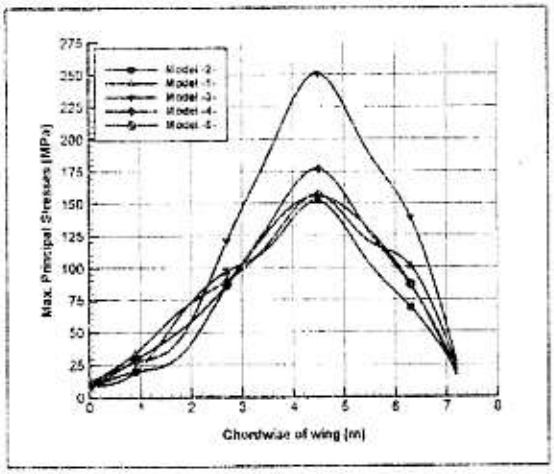

Fig. (14) Max. Principal stresses Vs chordwise (x) of delta wing (α=10°)

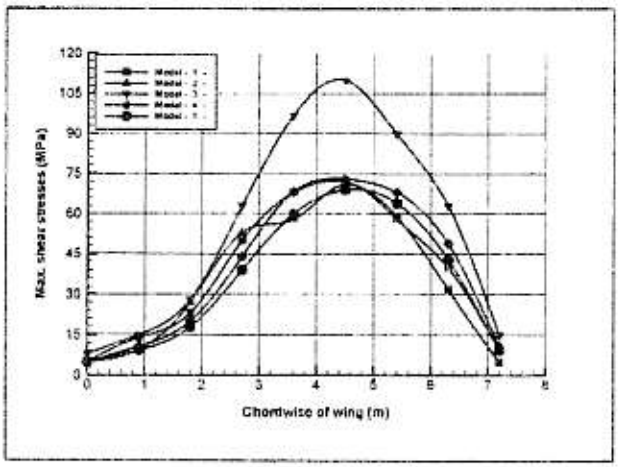

Fig. (15) Max. Shear stresses Vs chordwise (x) of delta wing (α=10°)

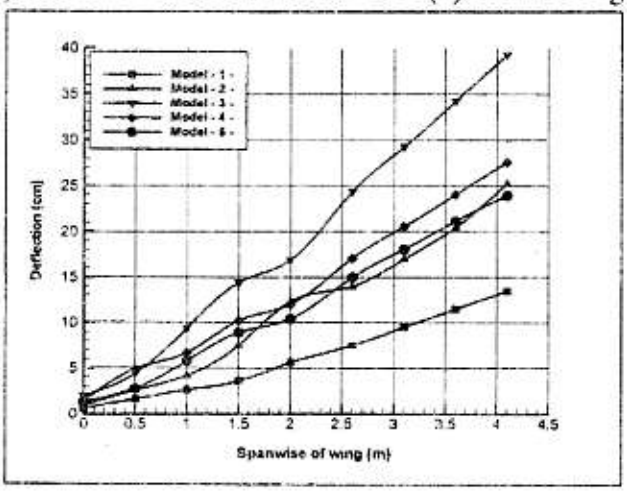

Fig. (16) Deflection Vs spanwise (y) of delta wing (α=10°)

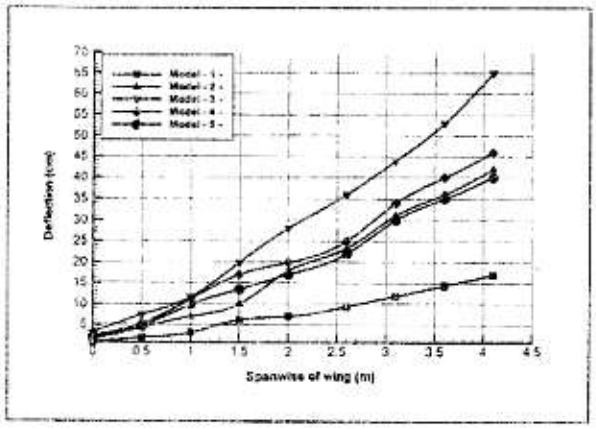

Fig. (17) Deflection Vs spanwise (y) of delta wing (α=12°)

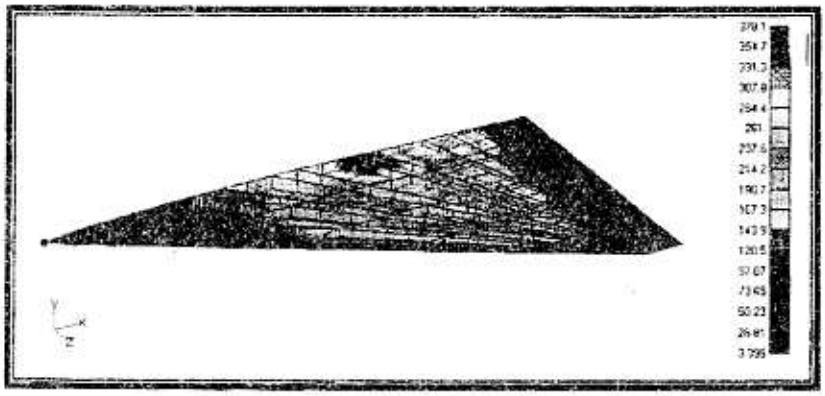

Figure (18) Von-Misses stress distribution (MPa) For wing design 2 at α=14°

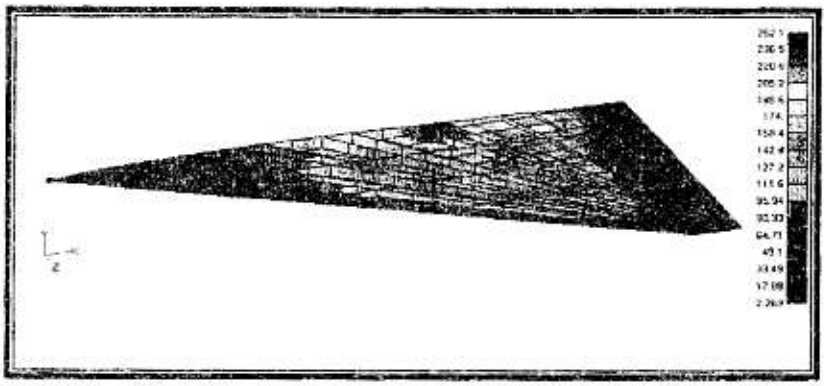

Figure (19) The Von-Misses stresses (MPa) for Wing design 2 at α=12°

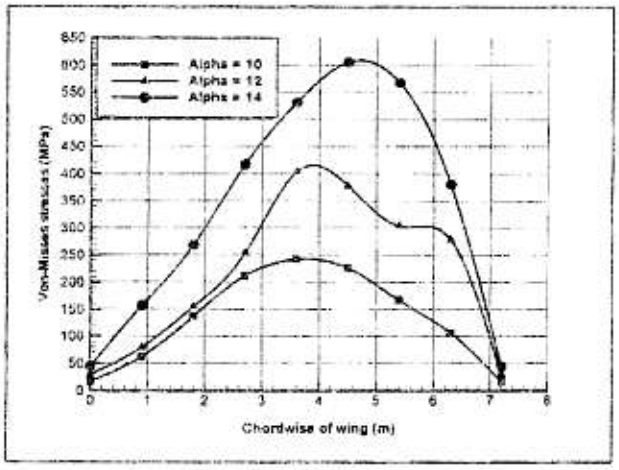

Fig. (20) Von-Misses stresses Vs chordwise (x) of wing design 3

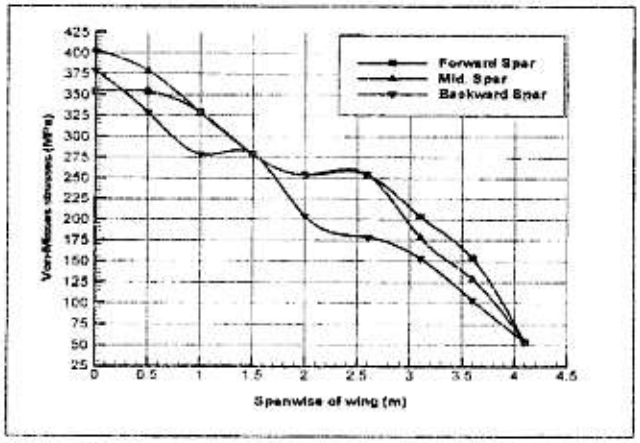

Fig. (21) Von-Misses stresses Vs spanwise (y) of wing design 3 (α=12°)

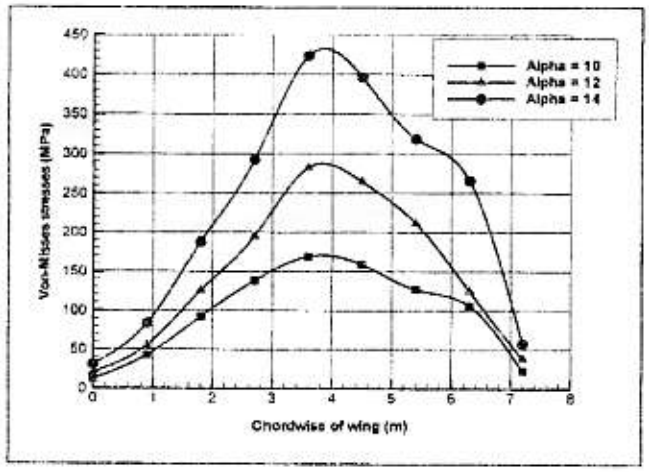

Fig. (22) Von-Misses stresses Vs chordwise (x) of wing design 4

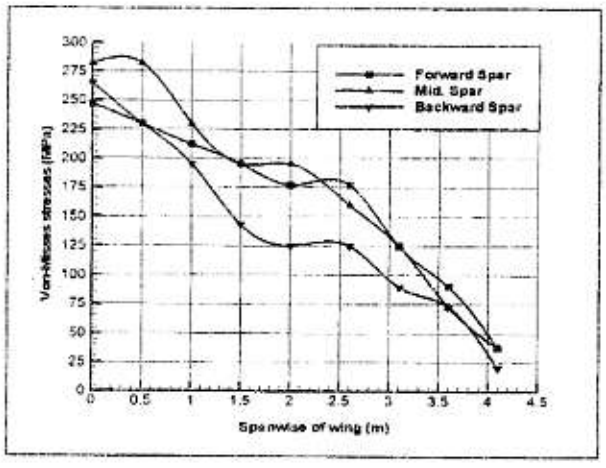

Fig. (23) Von-Misses stresses Vs spanwise (y) of wing design 4 (α=12°)

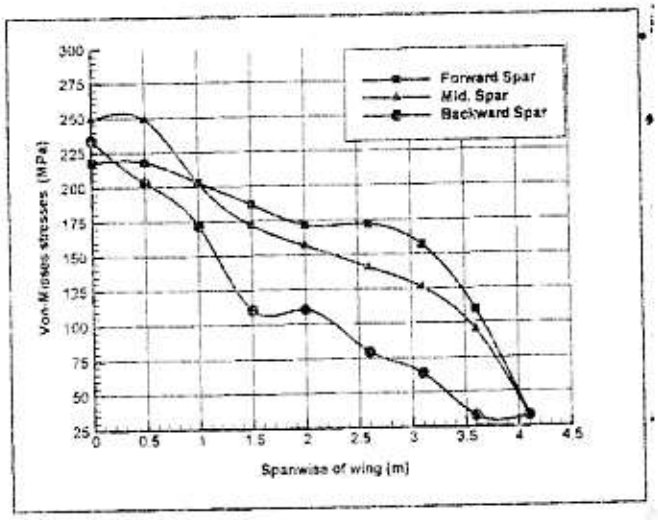

Fig. (24) Von-Misses stresses Vs spanwise (y) of wing design 5 (α=12°)